JOURNAL OF CATALYSIS **173,** 145–156 (1998)
ARTICLE NO. CA971874

Tailoring Alumina Surface Chemistry for Efficient Use of Supported MoS_2[1]

John Reardon, Abhaya K. Datye, and Allen G. Sault*

*Department of Chemical and Nuclear Engineering, University of New Mexico, Albuquerque, New Mexico 87131-1341; and *Catalysis and Chemical Technologies Department, Sandia National Laboratories, Albuquerque, New Mexico 87185-0710*

Received April 18, 1997; revised August 12, 1997; accepted August 14, 1997

Reported activity trends for hydrodesulfurization (HDS) over MoS_2/γ-Al_2O_3 catalysts show a maximum in activity with Mo loading when activity is normalized to Mo content. In contrast, simple monotonic decreases in normalized activity are observed over TiO_2 and ZrO_2 supports. While earlier work ascribes these different activity trends to differences in MoS_2 morphology, activity measurements and transmission electron microscope images presented here conclusively demonstrate that the two different trends can occur on support materials that give rise to virtually identical MoS_2 morphologies. Since differences in morphology cannot explain this result, we instead propose the following chemical explanation involving the formation of inactive molybdate species on γ-Al_2O_3 at low Mo coverages. Reaction of aqueous molybdates with the highest frequency, or type I-a, OH groups on γ-Al_2O_3 is known to form stable MoO_4^{2-} species at low Mo coverages, which are difficult to convert into the active MoS_2 form. As a result, normalized HDS activity is very low. As Mo coverage increases the type I-a OH groups are consumed and formation of more easily sulfided molybdate species begins to predominate, and normalized activity increases. Ultimately, normalized activity goes through a maximum with Mo coverage as the average size of the MoS_2 platelets begins to grow, resulting in a decrease in the fraction of Mo atoms located at active edge sites. Since the type-I-a hydroxyls on γ-Al_2O_3 are associated with tetrahedrally coordinated Al cations, it should be possible to prevent the formation of inactive molybdates, and thereby eliminate the maximum in activity with coverage, by removing all tetrahedrally coordinated Al cations from the surface. This removal has been accomplished through the use of α-Al_2O_3, which contains only octahedrally coordinated Al atoms, and through titration of the type I-a hydroxyls on γ-Al_2O_3 with titanium isopropoxide prior to Mo loading. In both cases, no maximum in activity is observed and activity at all Mo loadings is higher than on γ-Al_2O_3. Fourier transform infrared measurements of OH group consumption coupled with X-ray photoelectron spectroscopy measurements of molybdate reducibility support the chemical explanation by demonstrating that reaction of γ-Al_2O_3 with titanium isopropoxide preferentially consumes type I-a hydroxyls and that molybdates are more easily reduced on α-Al_2O_3 and titania coated γ-Al_2O_3 than on pure γ-Al_2O_3. Thus, titration of type I-a OH groups on γ-alumina by a suitable modifier, such as titania, offers a simple method for increasing the overall activity of supported MoS_2 catalysts, while retaining the advantageous properties of γ-Al_2O_3 supports, such as high surface area and thermal stability.

1. INTRODUCTION

MoS_2 based catalysts supported on γ-Al_2O_3 and promoted by Ni or Co are ubiquitous throughout the refining industry for removal of heteroatoms (S, N, metals) from petroleum feedstocks. These catalysts are frequently made by wet impregnation of γ-Al_2O_3 with metal salts, typically ammonium heptamolybdate and nickel or cobalt nitrates, followed by calcining and treatment in a sulfur containing stream (e.g., H_2S or a high sulfur oil) to convert the metal salts into sulfides. Despite the long history of these catalysts, much remains to be understood regarding their performance. This work aims to address one particular outstanding issue, namely, the effects of strong interactions between molybdates and the γ-Al_2O_3 surface that limit the conversion of Mo into the active sulfide form and consequently decrease catalytic activity.

For unpromoted MoS_2/γ-Al_2O_3 and MoS_2/SiO_2 catalysts, activity for thiophene hydrodesulfurization (HDS) is reported to proceed through a maximum with Mo loading when activity is reported on a Mo weight basis (1, 2). This maximum occurs at a Mo coverage of ~1.0 Mo atom/nm^2, corresponding to approximately 25% of the molybdenum monolayer limit (3, 4). Another report (5) claims that Mo/γ-Al_2O_3 catalysts exhibit virtually no activity for Mo coverages below 1.0 Mo/nm^2. In contrast, for MoS_2/TiO_2 and MoS_2/ZrO_2 catalysts a monotonic decrease in activity with Mo coverage occurs and activities per Mo atom at all loadings are higher than those on γ-Al_2O_3 or SiO_2 (1). Unfortunately, the low surface areas and thermal stabilities of titania and zirconia render them unsuitable for practical industrial use. Nevertheless, it is of interest to try to understand the differences in Mo–support interactions that give rise to the different activity trends, with an eye toward mitigating those effects that limit the activity of γ-Al_2O_3 supported catalysts.

[1] This work was supported by the United States Department of Energy under Contract DE-AC04-94AL85000. Sandia is a multiprogram laboratory operated by Sandia Corporation, a Lockheed Martin Company, for the United States Department of Energy.

0021-9517/98 $25.00

Based on an interpretation of transmission electron microscope (TEM) images, Pratt *et al*. (1) postulated that the different activity trends results from differences in MoS_2 morphology on the various supports, with TiO_2 and ZrO_2 giving rise to a basal plane morphology where the MoS_2 platelets orient parallel to the support surface and γ-Al_2O_3 and SiO_2 giving rise to a "bookend" morphology where the MoS_2 platelets orient perpendicular to the support surface. Recent work on low surface area model supports (6) casts doubt on this interpretation, however, and suggests that the apparent bookend morphology may simply be an artifact of the TEM observation. In this study, MoS_2 platelets in a basal plane morphology were unambiguously observed on all of the model support surfaces (SiO_2, δ-Al_2O_3, and TiO_2). The apparent observation of a bookend MoS_2 morphology on high surface area silica and alumina supports could arise from the presence of support surfaces that are perpendicular to the plane of the sample, but buried deep within the support. MoS_2 platelets bound in a basal plane morphology on such surfaces would be oriented perpendicular to the plane of the TEM grid and could therefore be mistaken for MoS_2 in the bookend morphology. Such an occurrence is especially likely on γ-Al_2O_3 because of the cubic structure of this material and its tendency to adhere to TEM grids with one crystal face parallel to the grid. In the case of titania and zirconia, the relatively low surface areas make observation of internal structures oriented perpendicular to the viewing direction unlikely, and MoS_2 platelets are observed only on external surfaces of the support particles where the basal plane morphology is clearly apparent. This conclusion is also consistent with the TEM studies of Delannay (7) and Payen *et al*. (8) who concluded that the only unambiguous morphology on γ-alumina is the basal plane orientation. In this paper we provide further evidence that a morphological explanation is not valid and that the reported bookend morphology is most likely the result of misinterpretation of TEM images.

If a morphological explanation of the different activity trends is rejected, then chemical explanations must be invoked. It is well known from infrared vibrational studies that γ-Al_2O_3 surfaces possess several different types of hydroxyl groups (9–12) and that during Mo loading aqueous molybdates react preferentially with the highest frequency (most basic) hydroxyl groups (11, 13, 14). The highest frequency hydroxyls with significant coverage on γ-Al_2O_3 have been identified as isolated OH groups singly bound to tetrahedrally coordinated aluminum cations (9) and labeled as type I-a hydroxyls (3770 cm^{-1}). Furthermore, Raman studies (3, 14–16) identify the initial Mo species formed at low Mo loadings as isolated tetrahedrally coordinated MoO_4^{2-}, while at higher loadings, polymolybdate species form that contain both tetrahedrally and octahedrally coordinated Mo(VI) ions. Ultimately, at Mo loadings above the monolayer limit, crystalline MoO_3 begins to form. X-ray photoelectron spectroscopy (XPS) studies show that the fraction of adsorbed molybdate that can be converted into MoS_2 under typical sulfiding conditions is far less at low molybdenum loadings ($<$1.0 Mo/nm^2) than at high molybdenum loadings ($>$3.0 Mo/nm^2) (17). Combining this information leads to the conclusion that inactive molybdate species (i.e., molybdates that are not readily converted into MoS_2) are formed upon reaction of aqueous molybdates with isolated, type I-a hydroxyl groups bound to tetrahedrally coordinated Al cations on the support surface. At low Mo coverages, these inactive species dominate and HDS activity normalized to Mo content is very low. As the Mo coverage increases, a greater fraction of the Mo adsorbs in the form of polymolybdates that are easily sulfided and normalized activity increases. As the loading increases above $\sim$1.0 Mo/nm^2, the fraction of the Mo that can be converted to MoS_2 becomes constant, but the average size of the MoS_2 platelets formed during sulfiding begins to increase, resulting in a drop in the fraction of Mo atoms located at the edges of the platelets. Since these edge sites are widely believed to be the active sites for HDS, normalized activity decreases above 1.0 Mo/nm^2. In contrast, on supports such as TiO_2 and ZrO_2 the hydroxyl groups present are not conducive to the formation of inactive Mo species and the activity trend is determined solely by growth in the average MoS_2 platelet size with Mo coverage, resulting in a monotonic decrease in normalized activity.

If the above hypothesis is true, then the formation of inactive molybdates on γ-Al_2O_3 could be prevented by eliminating the presence of tetrahedrally coordinated Al atoms from the support surface. One method of testing this hypothesis is through the use of α-Al_2O_3 as a support since, unlike γ-Al_2O_3 in which one-third of the Al cations occupy tetrahedral sites, all of the Al cations in α-Al_2O_3 occupy octahedral sites (18). A second method is to modify γ-Al_2O_3 in such a way that all of the type I-a hydroxyl groups are consumed prior to Mo loading. In either case, activity trends would be expected to shift from exhibiting a maximum in normalized activity with coverage to a monotonic decrease, and the activity at all coverages would be expected to increase. In this article both methods will be explored, and it will be demonstrated through a combination of HDS activity measurements and catalyst characterization that elimination of type I-a hydroxyl groups from γ-Al_2O_3 does indeed minimize the formation of inactive molybdate species and result in increased HDS activity at all Mo loadings.

2. METHODS

2.1. Support Preparation

Several different support materials were used for this study, including γ-Al_2O_3 (Criterion 324M support), α-Al_2O_3 (Sumitomo AKP-50), nonporous TiO_2, and TiO_2

coated γ-Al_2O_3. The Criterion γ-Al_2O_3 was chosen because it is also the support for Criterion 324, an industrial HDS catalyst containing 2.7% Ni, 13.2% Mo, and 3.2% P by weight. This particular γ-Al_2O_3 was obtained in the form of 1/16″ extrudates with a surface area of 236 m^2/g, a pore volume of 0.64 cc/g, a unimodal pore size distribution with average pore diameter of 108 Å, and a sodium content of 140 ppm. The α-Al_2O_3, obtained as a nonporous powder with a BET surface area of 10 m^2/g, contains trace impurities of Na (2 ppm), Mg (2 ppm), Si (5 ppm), and Fe (5 ppm).

A titania film was deposited onto dried, granulated (−60/+80 mesh) γ-Al_2O_3 by impregnation with a titanium isopropoxide solution (50 vol% Ti(i-OPr)$_4$ in hexane) in excess of the support pore volume in a dry argon atmosphere. After standing for 1 h, the slurry was filtered, washed twice with hexane, and dried overnight at room temperature under vacuum. The powder was then heated to 773 K in air at 5 K/min and held at 773 K for 4 h. This coating process was repeated two more times to give a final TiO_2 loading of 16.2% by weight, as determined by X-ray fluorescence (XRF). Based on an estimated TiO_2 monolayer capacity of 1.37×10^{-3} g/m^2 (19) and the γ-Al_2O_3 surface area of 236 m^2/g, 24.4 wt% TiO_2 would be required to completely cover the γ-Al_2O_3 surface. Hence, the measured TiO_2 loading of 16.2 wt% corresponds to at most 60% coverage of the γ-Al_2O_3 surface. XPS analysis of the TiO_2/γ-Al_2O_3 sample results in a Ti 2p/Al 2p intensity ratio of 2.0. Based on the method of Kerkhof and Mouljin (20) an expected ratio of 2.7 can be calculated. The slightly lower experimental value suggests some agglomeration of titania, but since no titania particles are observable by TEM, any agglomeration is assumed to be insignificant and the film is taken to be well dispersed. The titania coated γ-Al_2O_3 support material has a BET surface area of 207 m^2/g.

In addition to the titania coated γ-Al_2O_3, pure titania powder was also employed as a support material. A highly pure, nonporous TiO_2 powder was prepared by the method of Barringer and Bowen (21), using controlled precipitation from titanium ethoxide dissolved in an ethanol solution. The nitrogen BET surface area of the resulting TiO_2 is 22 m^2/g.

2.2. Molybdenum Loading

The γ-Al_2O_3 and TiO_2/γ-Al_2O_3 supports were ground to −200 mesh before Mo loading, while the TiO_2 and α-Al_2O_3 supports were loaded in their as-prepared and as-received conditions, respectively. Molybdenum was deposited on all supports by a method of equilibrium deposition–impregnation (EDI). A stock solution of aqueous ammonium heptamolybdate was diluted to varying degrees and an excess amount of solution was added to the support powder (typically 2 g). The resulting slurry was agitated for 30 min, centrifuged to sediment the powder, and decanted to remove excess solution. All the samples prepared in this manner were dried overnight at 378 K and calcined at 773 K for 1 h prior to characterization and sulfiding.

All samples were analyzed for Mo using either atomic absorption spectroscopy (AAS), energy dispersive spectroscopy (EDS), or XRF. AAS was the method of choice; however, in a few cases AAS results were verified by XRF or EDS. Samples were prepared for AAS by extracting the molybdenum from the supports in boiling, concentrated HCl. AAS was performed on a Perkin Elmer 5100 PC atomic absorption spectrophotometer. Samples were prepared for XRF by grinding and sieving to −200 mesh, mixing 5.00 wt% sample with lithium tetraborate, melting the mixture at 1273 K for 12 min, and pouring the melt into a smooth platinum mold to make the analyte disk. XRF measurements were made on a Rigaku 3064-M wavelength-dispersive X-ray fluorescence spectrometer with a rhodium target operated at 50 kV and 45 mA. EDS was performed on a JEOL 2010 microscope equipped with an Oxford instruments EDS system with a Link thin window detector. The results of the molybdenum deposition on the various supports are presented in Table 1.

2.3. HDS Activity Testing Procedure

2.3.1. Catalyst sulfiding. After calcining, all catalysts were presulfided *ex situ* prior to use. Catalysts were first pelletized by pressing at 1200 psi and then ground to −20 mesh. The catalyst samples were then sulfided inside a quartz tube inserted into a tube furnace. Sulfiding was performed at 693 K for 2 h under ∼25 sccm of a 10% H_2S/H_2 mixture. After sulfiding, the catalysts were cooled to 473 K in the H_2S mixture, flushed with helium, and cooled to room temperature. All catalysts were ground in a corundum mortar and pestle and sieved to −200 mesh before use. In order to minimize reoxidation of the *ex situ* sulfided catalysts, samples were tested as soon as possible after sulfiding, generally on the same day. Furthermore, it should be noted that even for the highest Mo loadings, the total amount of Mo present in the reactor is nearly two orders of magnitude less than the amount of DBT added to the reactor and that the observation of many MoS_2 particles during TEM analysis of the sulfided catalysts shows that at most a small fraction of the MoS_2 is reoxidized. Thus, any MoS_2 reoxidized during air exposure would be resulfided during activity testing without consuming a significant amount of the DBT.

2.3.2. HDS reactor testing. All catalytic activity tests were performed in a batch microautoclave reactor shown schematically in Fig. 1. The reactor consists of an end capped 1/2″ Cajon VCR tee attached to a 3/8″ OD stainless steel tube. The tube is connected to the outlet of a Whitey gauge valve (Model SS-4PDGF4). This valve has a second port across from the outlet to accommodate a type K (Cr−Al) thermocouple that extends into the VCR tee for temperature measurement and a third port that is used to monitor pressure. A hydrogen inlet port is present on the other

TABLE 1

Mo Content of Calcined Catalyst Samples

γ-Al_2O_3			TiO_2			α-Al_2O_3			TiO_2/γ-Al_2O_3		
Mo content[a] (wt% Mo)	Mo coverage[b] (Mo/nm^2)	Rate constant (mmol S/g-Mo/min)	Mo content[a] (wt% Mo)	Mo coverage[b] (Mo/nm^2)	Rate constant (mmol S/g-Mo/min)	Mo content[a] (wt% Mo)	Mo coverage[b] (Mo/nm^2)	Rate constant (mmol S/g-Mo/min)	Mo content[a] (wt% Mo)	Mo coverage[b] (Mo/nm^2)	Rate constant (mmol S/g-Mo/min)
0.93	0.25	—	0.135	0.39	17.7	0.038	0.24	—	0.66	0.20	—
2.88	0.80	1.51	(0.39)[c]	(1.12)[c]	6.32	0.069	0.44	12.3	1.62	0.50	6.4
3.69[d]	1.04[d]	1.69	0.52	1.49	5.25	0.187	1.19	4.67	3.39	1.08	3.41
4.51	1.28	1.79	0.72	2.08	4.41	0.349	2.20	2.78	4.98	1.63	3.91
6.14	1.8	1.56	1.04	3.01	3.02	0.463	2.92	2.59	6.40	2.35	2.39
8.01, 7.97[e]	2.42	—	1.44	4.18	1.88	0.537	3.40	2.5	11.54	4.24	1.45
12.73	4.19	0.77				0.667	4.25	1.96	(9.53)[e]	(4.76)[e]	1.24
13.78	4.62	0.82							15.70	6.23	1.04

[a] Unless noted Mo loading determined by AAS.

[b] Support surface areas of 236 m^2/g (γ-Al_2O_3), 22 m^2/g (TiO_2), 10 m^2/g (α-Al_2O_3), and 207 m^2/g (TiO_2/α-Al_2O_3) were used to calculate Mo surface densities (Mo/nm^2).

[c] Mo loading not measured, but estimated by interpolation on a plot of Mo loading vs impregnating solution concentration.

[d] Mo loading determined by calibrated EDS.

[e] Mo loading determined by XRF.

side of the valve. Total reactor volume is approximately 15 cm^3.

HDS testing was performed by adding presulfided catalyst (20 mg for γ-Al_2O_3 and TiO_2/γ-Al_2O_3, 90 mg for TiO_2 and α-Al_2O_3), 200 $\pm$ 2 mg of dibenzothiophene (DBT), and 2.6 ml of hexadecane solvent to the VCR tee. The reactor vessel was evacuated using a mechanical pump, and pressurized to 1200 psig with hydrogen. The reactor was then attached to a wrist action shaker and immersed into a fluidized sand bath preheated to 623 K. Each catalytic test was performed in duplicate by dipping two reactor vessels in the sand bath at a time. Total reaction time varied from 10 to 60 min depending on the Mo loading, after which the reaction was quenched by rapidly immersing the reactors in water. After quenching the reactors were depressurized and vented for ~10 min to remove H_2S. Reactants and products were removed from the VCR tee, reactor tube, and thermocouple using multiple toluene rinses and quantitatively collected in a 100-ml volumetric flask. One milliliter of internal standard solution (50 mg 2-methylnapthalene in 50 ml toluene) was added to the solution before diluting to 100 ml. The final solution was filtered through a 0.2-μm syringe filter system to separate the catalyst before GC analysis.

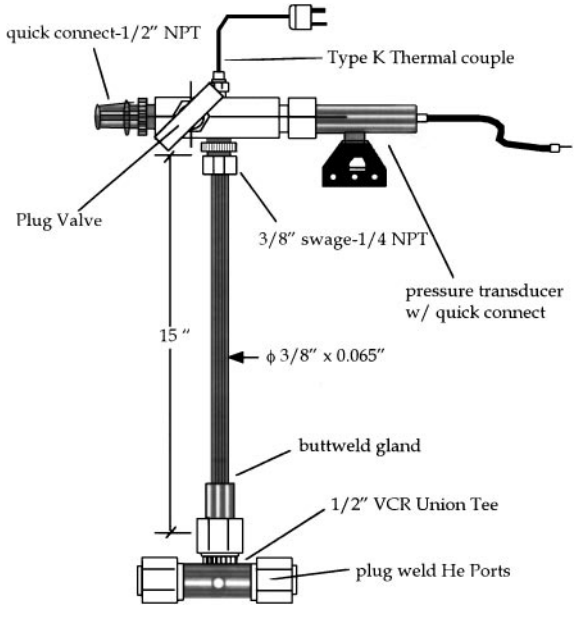

FIG. 1. Schematic diagram of batch microautoclave reactor.

GC analysis of the products was performed on an HP 5890 gas chromatograph equipped with a Carbowax capillary column and a flame ionization detector (FID). Relative response factors were determined with respect to 2-methylnaphthalene using an external standard. Mass balances indicate typical DBT recoveries of 80–90%. Since solvent recovery and DBT recovery are nearly identical; however, we assume that the reactor is well mixed and that the failure to achieve 100% recovery does not introduce any significant bias into the results.

2.3.3. Kinetic analysis. DBT conversion, as well as selectivity to the various products were calculated for all catalysts studied. Because of the large variations in surface area and Mo content among the catalysts, conversions ranging from negligible to nearly complete DBT consumption would be obtained if all catalysts were tested under

identical conditions. In order to avoid this situation and obtain conversions high enough to measure accurately, but not approaching complete consumption of DBT, different reaction times, and/or catalyst quantities were used for each measurement. Also, using the batch reactor, only a single data point was obtained for each catalyst rather than a plot of conversion vs time. Measuring conversion as a function of time for each catalyst would be extremely time intensive. For these reasons, a simple comparison of conversion over the various catalysts under identical reaction conditions is not possible, nor is it possible to extrapolate rates from the slopes of conversion vs time plots. Instead, a kinetic analysis must be made that allows determination of an accurate rate constant from a single conversion/time data point. This kinetic analysis is quite involved and will therefore not be presented in detail here. Complete details are available elsewhere (22). The kinetic analysis is based on a series of measurements of DBT conversion vs time over a commercial HDS catalyst (Criterion 324M). The assumed reaction pathway, taken from work by several groups (23–26), produces biphenyl (BP) by direct desulfurization of DBT, and cyclohexylbenzene (CHB) by hydrogenation of DBT to tetrahydrodibenzothiophene (H_4DBT) followed by desulfurization of H_4DBT to CHB. Secondary hydrogenation of BP is not important in this scheme and DBT and H_4DBT are assumed to be in equilibrium on the surface (i.e., HDS of H_4DBT is the rate limiting step in CHB production). A first order plot of ln[DBT] vs time for the Criterion 324 catalyst results in a fairly straight line, but such an analysis is inconsistent with published kinetics that use a zero order model (23). A simple zero order model does not fit the Criterion 324 data satisfactorily, however, most likely due to the buildup of H_2S in the batch reactor and a resulting suppression of DBT and H_4DBT adsorption through competition with the H_2S. This H_2S buildup is absent in flow reactor studies that use flowing hydrogen to sweep product gases out of the reactor (23). Consequently, competitive adsorption of H_2S has been added to the zero order kinetic model used here, resulting in the HDS rate expression (22),

$$\begin{aligned}\text{Rate}_{\text{HDS}} &= \frac{N_{\text{A0}}}{m_{\text{cat}}}\frac{\text{d}(X_{\text{H}_2\text{S}})}{\text{d}t}\\ &= k_{\text{HDS}}\frac{\alpha - X_{\text{HDS}}}{\alpha + \alpha((K_{\text{H}_2\text{S}}/K_{\text{DBT}}) - 1)X_{\text{HDS}}},\end{aligned}$$

where N_{A0} is the initial moles of DBT, m_{cat} is the mass of catalyst $X_{\text{H}_2\text{S}} = X_{\text{HDS}}$ is the sum of the conversions to CHB and BP, α is the HDS selectivity ($X_{\text{CHB}} + X_{\text{BP}}/X_{\text{CHB}} + X_{\text{BP}} + X_{\text{H}_4\text{DBT}}$), and K_x is the equilibrium constant for adsorption of species X. No significant changes in hydrogen pressure are observed during reaction, so the hydrogen dependency is lumped into the rate constant. Experimentally, α is found to be fairly constant with conversion for the Criterion 324 catalyst, allowing the rate equation to be integrated and fit to the data for Criterion 324, resulting in a value of 2.75 for the ratio of the equilibrium adsorption constants, $K_{\text{H2S}}/K_{\text{DBT}}$. Using this value for the experimental catalysts allows k_{HDS} to be determined from a single conversion measurement. In addition to the kinetic analysis, the effects of temperature transients during immersion of the reactors in the sand bath is accounted for using measurements of the temperature vs time profile during startup, and an activation energy for HDS of 39 kcal/mol (27). The net result of this analysis is the determination of a zero-order rate constant for DBT HDS, k_{HDS}, that requires only a *single* measurement of DBT conversion, HDS selectivity, and reaction time. It is important to note that while we believe this kinetic analysis to be accurate and necessary to obtain quantitatively correct zero order rate constants, qualitatively similar activity trends do result from simple first order or zero order models, even though these models cannot accurately fit the conversion vs time data for the commercial catalyst. Thus, the overall conclusions of this paper are independent of the actual kinetic model used.

2.4. Infrared Absorption Spectroscopy

A Nicolet 20SXB Fourier transform infrared spectrometer equipped with a SpectraTech COLLECTOR diffuse reflectance accessory and high temperature/vacuum chamber was used to obtain infrared spectra of the catalysts. Samples were prepared by grinding and sieving the calcined catalysts to −80 mesh and then mixing with separately ground KBr powder to form a sample containing 10 wt% catalyst. Background spectra were taken from pure ground KBr. The sample cup was loosely filled with the catalyst/KBr mixture (or pure KBr for background acquisition) and leveled by running a straight edge across the top of the sample cup. The sample chamber was then sealed and purged with flowing UHP nitrogen at room temperature until the absorption peaks of water were eliminated, typically around 1 h. The sample cell was then heated in flowing nitrogen to 473 K and held for ∼60 min until no further dehydroxylation of the sample was apparent by FTIR over a 15-min period. A full spectrum was then taken and the procedure was repeated at 600 and 750 K. All spectra were taken with a resolution of 4 cm^{-1} and a total of 2048 scans, for a data acquisition time of ∼15 min.

2.5. X-Ray Photoelectron Spectroscopy

XPS measurements were made in a combined ultrahigh vacuum (UHV) surface analysis/atmospheric pressure reactor system (28, 29) that allows measurement of the surface properties of catalytic materials before and after exposure to reactive environments without intervening exposure to air. Using this system, measurements of Mo surface concentrations and Mo oxidation states were made for each calcined catalyst after heating to 773 K in vacuum for 5 min, and after reduction in 630 Torr hydrogen at 773 K for 4, 8,

and 12 h. Spectra were taken using a nonmonochromatic Mg $K\alpha$ source with an analyzer resolution of 1.0 eV. As discussed below, this measurement provides an indication of the fraction of the surface molybdate species that can be converted into active MoS_2 during sulfiding. Because of the insulating nature of the supports, some sample charging always occurred and binding energies were referenced to the Al 2p peak at 74.1 eV (30, 31). In the case of the TiO_2/γ-Al_2O_3, differential charging was often observed following hydrogen reduction, presumably induced by partial reduction of the TiO_2 overlayer. This differential charging was eliminated by biasing the sample with a positive voltage of 5–20 V until the broad Al 2p peak coalesced into a single sharp band (32).

Mo 3d spectra were subjected to Tougaard background subtraction and peak fitting using the routines included in the VGX900 software package that controls the spectrometer. The fitting procedure forces the widths of the Mo $3d_{5/2}$ and $3d_{3/2}$ peaks to be equal and fixes the heights of the $3d_{3/2}$ peaks at two-thirds of the corresponding $3d_{5/2}$ peak. Prior to any temperature or hydrogen treatments, all samples display a single Mo 3d doublet with a $3d_{5/2}$ binding energy of ~232.6 eV, and spin-orbit splitting of 3.1–3.2 eV, typical of Mo(VI) (15, 31). Spectra from reduced samples invariably display multiple Mo oxidation states. In most cases the use of two Mo 3d doublets results in acceptable fits, although on occasion the inclusion of a third doublet improves the fit somewhat. Repeated fits on a given spectrum, as well as fits of multiple Mo 3d spectra taken from the same sample indicate a precision of <4% for the fraction of Mo(VI) converted to Mo(IV) and ~0.1 eV for the Mo $3d_{5/2}$ peak positions.

2.5. Transmission Electron Microscopy

Electron microscopy was performed with a JEOL 2010 microscope equipped with a Oxford instruments EDS system with a Link thin window detector. Samples were prepared for TEM by dipping a holey carbon coated copper grid into the catalyst powder and shaking off any excess.

3. RESULTS AND DISCUSSION

3.1. HDS Activity

HDS activities for γ-Al_2O_3 and titania supported MoS_2, normalized to Mo content, are plotted as a function of Mo surface coverage in Fig. 2 and tabulated in Table 1. The data for both supports agree qualitatively with the results of Pratt *et al*. (1). On γ-Al_2O_3 the data display a maximum in activity near a coverage of 1.0 Mo/nm^2, while on the TiO_2 support a monotonic decrease in activity with coverage occurs. Because of differences in reaction conditions and the fact that Pratt *et al*. studied thiophene rather than dibenzothiophene, no comparison of absolute rates can be made. Nevertheless, the observation of similar activity trends in both cases indicates that these trends are a general property of HDS reactions on γ-Al_2O_3 and TiO_2 supported MoS_2 and are not specific to a single sulfur containing molecule. Because of the extremely low activity of the 0.25 Mo/nm^2/γ-Al_2O_3 catalyst it was not possible to obtain a reliable rate constant for this material to confirm that activity continues to decline below 0.8 Mo/nm^2. It is apparent, however, from the data of Pratt *et al*. (1), Bachelier *et al*. (2), and de Beer *et al*. (5) that activity does continue to decline below 0.8 Mo/nm^2, ultimately approaching zero. Note also that using the batch reactor system employed here, it is possible to extend the data for TiO_2 supported MoS_2 to lower coverages than in the study of Pratt *et al*. and thereby confirm that the monotonic decrease reported by Pratt *et al*. does in fact extend to coverages well below those at which the maximum is observed for γ-Al_2O_3. These initial activity measurements confirm that the batch reactor system employed here is capable of reproducing activity trends observed in earlier work and actually presents an important advantage over flow reactor studies by allowing studies of low surface area materials with low Mo coverages. Even so, it was not possible to obtain reliable rate constants for the lowest Mo loadings (<0.4 Mo/nm^2) on any of the samples.

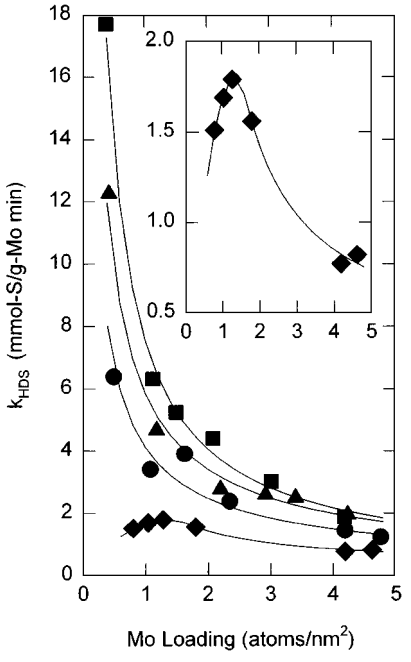

FIG. 2. Zero order rate constants as a function of Mo coverage for various supports: ◆, γ-Al_2O_3; ●, TiO_2/γ-Al_2O_3; ▲, α-Al_2O_3; ■, TiO_2. (Inset) Expanded plot of data for Mo/γ-Al_2O_3 that more clearly demonstrates the maximum in activity near 1.0 Mo/nm^2.

Armed with the knowledge that the batch reactor system is capable of reproducing published results, the activity studies were extended to α-Al_2O_3 and titania coated γ-Al_2O_3 supports. The data presented in Fig. 2 show very similar trends for the two supports. In both cases a simple

monotonic decrease with coverage is observed and the activity is higher than on γ-Al_2O_3 at all Mo coverages studied. These trends are in complete agreement with predictions based on the arguments presented in the Introduction and provide strong evidence implicating the role of type I-a hydroxyl groups in the formation of inactive Mo species on γ-Al_2O_3 surfaces. In order to confirm this hypothesis, however, physical evidence is needed to supplement the activity measurements.

3.2. FTIR

In order to determine whether the removal or absence of type I-a hydroxyls is responsible for changes in the HDS activity trends, FTIR measurements of the hydroxyl stretching region as a function of Mo coverage and support identity were employed. Spectra taken in the OH stretching region of the pure γ-Al_2O_3 support as a function of temperature agree well with numerous literature reports (9–12). Heating to 600 K results in recombination of associated hydroxyl groups and reveals the presence of three features arising from isolated hydroxyl groups (Fig. 3). Two of these features, at 3680 and 3730 cm^{-1}, are fairly well resolved, while the third feature, at 3770 cm^{-1} appears as a poorly resolved but very reproducible shoulder. It is this latter feature that is of interest here, having been identified as arising from the type I-a hydroxyl groups, i.e., those hydroxyl groups bound to tetrahedrally coordinated aluminum atoms (9). Heating to higher temperatures does not result in any further resolution of the isolated OH bands and in fact appears in many cases to result in some loss of intensity in these bands, with losses in the 3770 cm^{-1} band particularly noticeable. For this reason, all further spectra in this article will be reported after heating to 600 K.

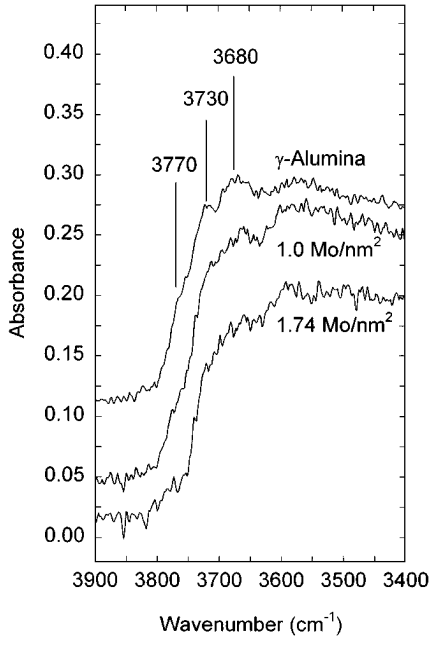

FIG. 3. FTIR spectra of the OH stretching region of γ-Al_2O_3 with various Mo coverages. All spectra taken after heating to 600 K.

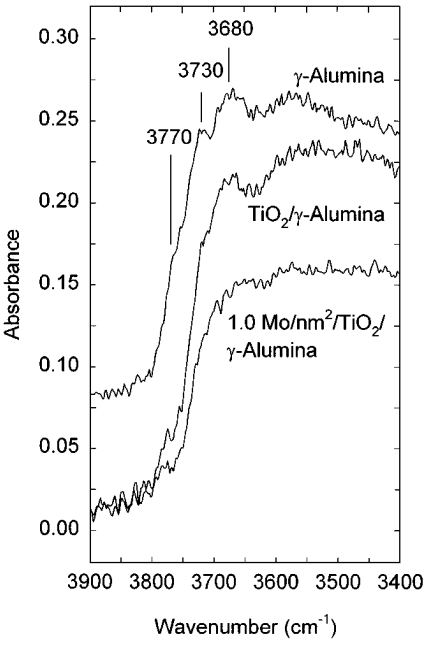

FIG. 4. FTIR spectra comparing the OH stretching region of γ-Al_2O_3 with TiO_2/γ-Al_2O_3 and 1.0 Mo/nm^2 on TiO_2/γ-Al_2O_3. All spectra taken after heating to 600 K.

Figure 3 shows the effects of low Mo coverages on the OH stretching bands. Concentrating only on the three isolated OH bands at 3680, 3730, and 3770 cm^{-1} reveals a preferential attenuation of the 3770 cm^{-1} (type I-a) band during the addition of Mo. At a coverage of 1.0 Mo/nm^2 this band shows a modest loss in intensity, but is almost completely attenuated at a coverage of 1.74 Mo/nm^2. In contrast, the 3680 and 3730 cm^{-1} bands are virtually unaffected in the 1.0 Mo/nm^2 sample and only slightly attenuated in the 1.74 Mo/nm^2 sample. The preferential attenuation of the highest frequency OH band during the addition of Mo is in excellent agreement with literature reports (13, 14). In fact, conversion of literature data from weight loading to Mo coverage (using reported surface area measurements) shows that Mo coverages of ~2 Mo/nm^2 are necessary to completely attenuate the 3770 cm^{-1} band, in excellent agreement with the current results.

Figure 4 shows the effects of the titania coating on the γ-Al_2O_3 support. The 3770 cm^{-1} shoulder is strongly attenuated by the titania overlayer, the 3730 cm^{-1} peak appears to be slightly attenuated, and the 3680 cm^{-1} peak is virtually unchanged. When the titania coated γ-Al_2O_3 is loaded with 1.0 Mo/nm^2, the result is total consumption of the remaining type I-a hydroxyls and a severe attenuation of both the 3680 and the 3730 cm^{-1} bands. Comparing this behavior to that of the uncoated γ-Al_2O_3 support (Fig. 3), where a coverage of 1.0 Mo/nm^2 has virtually no effect on the 3680 or

3730 cm^{-1} hydroxyls, shows that prior consumption of type I-a hydroxyls by the titania overlayer forces molybdate species to bind at sites associated with lower frequency hydroxyls. This demonstrated change in molybdate binding site coupled with the different activity trend and overall higher activity strongly supports the hypothesis that the type I-a hydroxyls are responsible for the formation of inactive Mo species.

It might be argued that with titania present on the γ-Al_2O_3 surface, the molybdate species are simply binding to the titania overlayer and not to the uncoated γ-Al_2O_3 surface. As a result, the activity trend of the titania coated γ-Al_2O_3 resembles that of bulk titania rather than that of γ-Al_2O_3. Based on the FTIR results, however, it appears that the deposition of titania consumes type I-a hydroxyls without producing additional hydroxyl bands attributable to titania (although titania bands at 3650, 3672, and 3716 cm^{-1} (33, 34) might be difficult to detect in the presence of the 3680 and 3730 cm^{-1} γ-Al_2O_3 bands), and that loading of the titania coated γ-Al_2O_3 with molybdates further consumes hydroxyl groups associated with the alumina surface. Furthermore, the isoelectric point of alumina is much higher than that of titania (7.0 vs 5.2 (22, 35)), suggesting that the γ-alumina surfaces should be more positively charged than the titania surfaces and that molybdate adsorption should therefore occur preferentially on the uncoated portions of the γ-Al_2O_3 surface. Based on these arguments, we conclude that the activity measurements made on the titania coated γ-Al_2O_3 are typical of molybdates adsorbed on modified γ-Al_2O_3 surfaces lacking type I-a hydroxyls and are not simply due to molybdates adsorbed on the titania coating. This issue will be further clarified by a systematic study of HDS activity as a function of titania coverage underway in our laboratories.

3.3. *X-Ray Photoelectron Spectroscopy*

While the activity measurements and FTIR results provide strong evidence that consumption of type I-a hydroxyls on γ-Al_2O_3 by titania and the absence of type I-a hydroxyls in α-Al_2O_3 both greatly enhance HDS activity and eliminate the activity maximum found on γ-Al_2O_3, the assumption that this enhancement is due to greater reducibility of adsorbed molybdates (i.e., easier conversion to MoS_2) must still be demonstrated. In order to make this demonstration the technique of Zingg *et al.* (15) was employed, whereby the extent of reduction of Mo(VI) to Mo(V) and Mo(IV) is measured during hydrogen reduction at 773 K. By comparison with the reduction behavior of MoO_3 and $Al_2(MoO_4)_3$ Zingg *et al.* deduced that octahedrally coordinated Mo(VI) is reduced to Mo(IV), while tetrahedrally coordinated Mo(VI) is reduced to Mo(V). In a related paper, Li and Hercules (17) demonstrated that treatment in a 10% H_2S/H_2 mixture at 623 K converts octahedrally coordinated Mo(VI) to MoS_2, while tetrahedrally coordinated Mo(VI) converts to a mixture of MoS_2 and Mo(V). The formation of Mo(V) is attributed to isolated (monomeric) tetrahedral Mo(VI) while formation of MoS_2 is attributed to dimeric tetrahedral Mo(VI). Thus, hydrogen reduction at 773 K provides a lower limit on the fraction of the Mo(VI) that can be converted into MoS_2. In spite of this limitation, hydrogen reduction was used here rather than H_2S treatments in order to avoid long-term contamination of the reaction chamber attached to the XPS spectrometer. Note also that hydrogen reduction should give qualitatively correct trends regarding the relative amounts of Mo(VI) that can be converted to MoS_2 (compare Fig. 9 in Ref. (17) with Fig. 8 in Ref. (15)) and therefore allow an accurate assessment of the relative ease of MoS_2 formation in the various catalysts.

Figure 5 shows the Mo 3d XP spectra obtained from the 1.19 Mo/nm^2/α-Al_2O_3 sample as a function of hydrogen reduction time. Initially, only Mo(VI) is detected, and heating in vacuum to 773 K for 5 min does not alter the oxidation state. This result is not typical of all samples; for high Mo loadings on α- and γ-Al_2O_3 heating in vacuum results in partial reduction to Mo(V), while for all loadings on the TiO_2 coated γ-Al_2O_3 reduction to a mixture of Mo(V) and Mo(IV) occurs. The extents of reduction to Mo(IV) are minor, however, compared to the reduction levels after hydrogen treatment. It is apparent in Fig. 5 that little change in Mo(IV) content occurs after 8 h of hydrogen reduction,

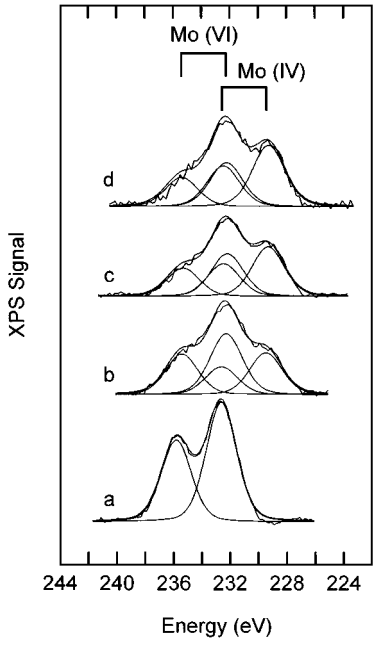

FIG. 5. Mo 3d XPS of 1.19 Mo/nm^2/α-Al_2O_3 sample in the as-prepared state (a), and after reducing in 630 Torr hydrogen at 773 K for (b) 4 h, (c) 8 h, (d) 12 h. Mo $3d_{5/2}$ and $3d_{3/2}$ peaks for both Mo(IV) and Mo(VI) components of the spectra, determined from the peak fitting procedure described in the text, are also shown.

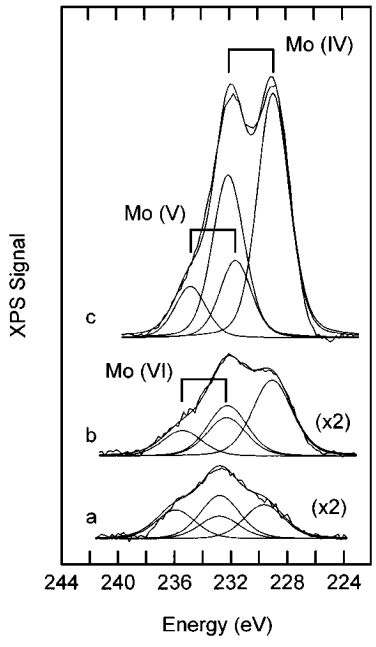

FIG. 6. Mo 3d XPS of Mo/γ-Al_2O_3 samples after reduction in 630 Torr hydrogen at 773 K for 12 h: (a) 0.25 Mo/nm^2, (b) 1.0 Mo/nm^2, and (c) 4.19 Mo/nm^2. Mo $3d_{5/2}$ and $3d_{3/2}$ peaks for the various components of the spectra, determined from the peak fitting procedure described in the text, are also shown.

a result typical of all of the samples studied here, as well as the samples studied by Zing *et al.* (15). Thus, the extent of reduction to Mo(IV) after 12 h is taken to be an indication of the fraction of Mo(VI) in octahedral coordination.

Figure 6 shows the XP spectra obtained from all of the Mo/γ-Al_2O_3 samples studied after reduction in hydrogen at 773 K for 12 h. Visual inspection clearly shows that the extent of reduction to Mo(IV) increases with Mo loading. Mo 3d peak fitting results are given in Table 2 for all supports and Mo loadings. The data clearly show that the extent of reduction to Mo(IV) increases with coverage for the γ-Al_2O_3 support, from a minimum of 40% for the 0.25 Mo/nm^2 sample, to a maximum of 75% for the 4.19 Mo/nm^2 sample. In contrast, the extent of reduction on α-Al_2O_3 is more nearly constant with coverage, increasing from 60% for coverages up to 1.19 Mo/nm^2 to 80% for a coverage of 4.25 Mo/nm^2. Finally, the extent of reduction is very high at ~75–80% for all TiO_2/γ-Al_2O_3 supported samples. These data clearly support the hypothesis that at low loadings on γ-Al_2O_3 most of the Mo(VI) is in a chemical state that is difficult to reduce, while on α-Al_2O_3 and titania coated γ-Al_2O_3 a much larger fraction of the Mo(VI) is reducible to Mo(IV) at low loadings. The ease of reducibility at low loadings therefore increases in the order γ-Al_2O_3 < α-Al_2O_3 < TiO_2/γ-Al_2O_3, while at high Mo loadings there is very little difference in reducibility among the three supports. Thus, XPS supports the hypothesis that the maximum in activity observed on γ-Al_2O_3 at low Mo loadings is related to formation of a Mo(VI) species that is difficult to reduce, while such a species does not form on α-Al_2O_3 or TiO_2 coated γ-Al_2O_3. The differences in activity at high Mo coverages are not explained by differences in Mo reducibility, nor is the higher activity of α-Al_2O_3 relative to TiO_2/γ-Al_2O_3 at low Mo coverages (12.3 vs 6.4 mmol DBT/g-Mo minute) given the slightly lower extent of reduction on α-Al_2O_3 (60% vs 75%). In this regard, it should be remembered that hydrogen reduction provides only a lower limit on the fraction of Mo that can be converted to MoS_2. It is therefore possible that a higher fraction of the tetrahedral Mo (which is not reduced in hydrogen (15)) can be converted into MoS_2 on α-Al_2O_3 than on TiO_2/γ-Al_2O_3. Since the hydrogen reduction experiments indicate that at least 75% of the Mo(VI) can be converted to MoS_2 on the TiO_2/γ-Al_2O_3 support, such a difference could account for at most a difference of 25% in the activities on the two supports and not the observed factor of two. A similar argument can be applied to explain partially the difference

TABLE 2

Summary of XPS Results for Hydrogen Reduced Samples

Support	Mo loading (Mo/nm^2)	Mo/Al intensity ratio (×4)	% Reduction to Mo(IV)[a]	Mo(IV)/Al intensity ratio	Mo(IV) BE (eV)	2nd component BE (eV)	ΔBE[b]
γ-Al_2O_3	0.25	0.47	40	0.19	229.6	232.7	3.1
γ-Al_2O_3	1.04	0.75	62	0.47	229.0	232.2	3.2
γ-Al_2O_3	4.19	5.1	75	3.8	228.8	231.5	2.7
α-Al_2O_3	0.24	0.25	58	0.15	229.1	232.9	3.8
α-Al_2O_3	0.44	0.46	61	0.29	229.4	232.9	3.5
α-Al_2O_3	1.19	1.2	60	0.72	229.1	232.2	3.0
α-Al_2O_3	4.25	2.9	80	2.32	228.9	231.7	2.8
TiO_2/γ-Al_2O_3	0.20	0.95	79	0.75	228.3	230.8	2.5
TiO_2/γ-Al_2O_3	0.50	2.7	74	2.0	228.8	231.6	2.8
TiO_2/γ-Al_2O_3	4.24	6.5	75	4.9	228.6	231.0	2.4

[a] Determined after reduction in 630 Torr hydrogen at 773 K for 12 h.
[b] Difference in binding energy between the Mo $3d_{5/2}$ peaks of the two Mo species present.

in activity between high Mo loadings on γ-Al_2O_3 and the other two supports, but as before, this effect could account for at most a 25–35% difference. A more likely explanation for the differences between the low loading α-Al_2O_3 and TiO_2/γ-Al_2O_3 samples is that differences in MoS_2–support interactions result in formation of larger MoS_2 platelets for a given Mo loading on TiO_2/γ-Al_2O_3 than on α-Al_2O_3. While such differences in MoS_2 platelet size might also explain the activity differences among the high Mo loading samples, a second possible explanation will be presented during discussion of the TEM data below.

Some additional comments on the XPS results, summarized in Table 2, are in order at this point. First, while the lowest binding energy component in all samples is identified as Mo(IV), there is considerable variation in the position of this peak. This variation is attributed to an absence of strong coupling between the Fermi levels of the support and the Mo(IV) species, particularly in the case of the TiO_2/γ-Al_2O_3 support, where Mo(IV) binding energies are well below the reported literature values of 229.1 to 229.4 eV (15, 31). The binding energies of the second Mo component also vary widely, but because of the variations in the Mo(IV) binding energy, it is most useful to compare the differences in binding energies between the two components. Based on reported values of 232.4 to 232.7 eV for Mo(VI) (15, 31), a binding energy difference of 3.0 to 3.6 eV is expected between Mo(VI) and Mo(IV), while based on reported binding energies of 231.6 to 231.9 eV for Mo(V) on γ-Al_2O_3 (17, 36) a binding energy difference of 2.2 to 2.8 eV is expected between Mo(V) and Mo(IV). Thus, for both α- and γ-Al_2O_3 the identity of the second component shifts from predominantly Mo(VI) to predominantly Mo(V) as the loading increases. In contrast, Zingg *et al.* found only Mo(V) as the second component on γ-Al_2O_3 for all Mo coverages. This difference is likely due to differences in chemical behavior between the γ-Al_2O_3 samples used in the two studies. Note also, that the gradual shift in second component binding energy with loading suggests that both Mo(V) and Mo(VI) are present in samples with intermediate loadings. Curve fitting using three Mo oxidation states did not significantly improve the fits, however, so only the simpler two component fits are reported. For the TiO_2/γ-Al_2O_3 samples, Mo(V) appears to be the second component for all loadings.

Second, comparison of Mo 3d/Al 2p intensity ratios with Mo loadings shows an excellent linear correlation for α-Al_2O_3, indicating that the Mo is uniformly dispersed. For γ-Al_2O_3 and TiO_2/γ-Al_2O_3 the correlation is much poorer, particularly at the highest loadings where the ratios are much lower than expected relative to the lowest loading samples. This result suggests that Mo is not uniformly dispersed and may be preferentially located on the outside of the porous particles at the lower loadings. Such a result could occur if, during Mo loading, aqueous Mo species are strongly attracted to adsorption sites near pore mouths in the support and insufficient time is allowed for these species to migrate into the pores and reach equilibrium with all of the sites on the support. For the highest Mo loadings ($\sim$4.25 Mo/nm^2), which are approximately equal to the monolayer limit for Mo, all adsorption sites near the pore mouths are consumed early in the adsorption process and additional Mo species must migrate into the pores to find available adsorption sites. As a result, virtually all Mo adsorption sites are used and a fairly uniform Mo distribution occurs. In the case of α-Al_2O_3 this effect is not seen since the support consists of dense, low surface area particles with very little porosity, and all adsorption sites are equally accessible.

3.4. Transmission Electron Microscopy

Figure 7 shows TEM images of high Mo loadings on both γ-Al_2O_3 and TiO_2/γ-Al_2O_3 after sulfiding. The morphology of the MoS_2 platelets is essentially identical for the two supports; mainly single layers of MoS_2 are distributed fairly uniformly throughout the samples. Thus, regardless of whether these images are interpreted as evidence for a bookend MoS_2 morphology, these images provide conclusive proof that morphological differences cannot explain the different activity trends observed on the two supports. Furthermore, upon close inspection of the images it can be seen that the MoS_2 fringes most often outline γ-Al_2O_3 grains. Coupled with an earlier study on δ-alumina spheres (6), where only the basal plane morphology was observed, this result provides strong evidence that MoS_2 is adsorbed in a basal plane morphology even on γ-Al_2O_3 and that earlier interpretations of these images as evidence for a bookend morphology are due to a failure to account for the internal structure of the high surface area γ-Al_2O_3 materials.

An important aspect of the TEM images is that small (1 nm) dots are apparent in the γ-Al_2O_3 image but not in the TiO_2/γ-Al_2O_3 image. These dots appear at all Mo loadings on γ-Al_2O_3, even with loadings so low that MoS_2 fringes are difficult to detect, but are never observed on TiO_2/γ-Al_2O_3. Also, the dots tend to grow under the influence of the imaging electron beam. These dots are attributed to a reduced phase of Mo formed from an unsulfided Mo(VI) or Mo(V) phase during imaging. Along with potential differences in MoS_2 platelet size, the presence of such unreduced molybdates could help to explain why XPS detects similar extents of reduction for high Mo loadings on all supports even though the activity over γ-Al_2O_3 is a factor of two less than on TiO_2/γ-Al_2O_3. If this unreduced molybdate phase is present as large particles or a relatively thick film (2–3 nm), the photoelectron signal from this phase would be attenuated, while the signal from the reduced Mo(IV) phase, assumed to be well dispersed, would be unattenuated. In such a situation, XPS would measure an extent

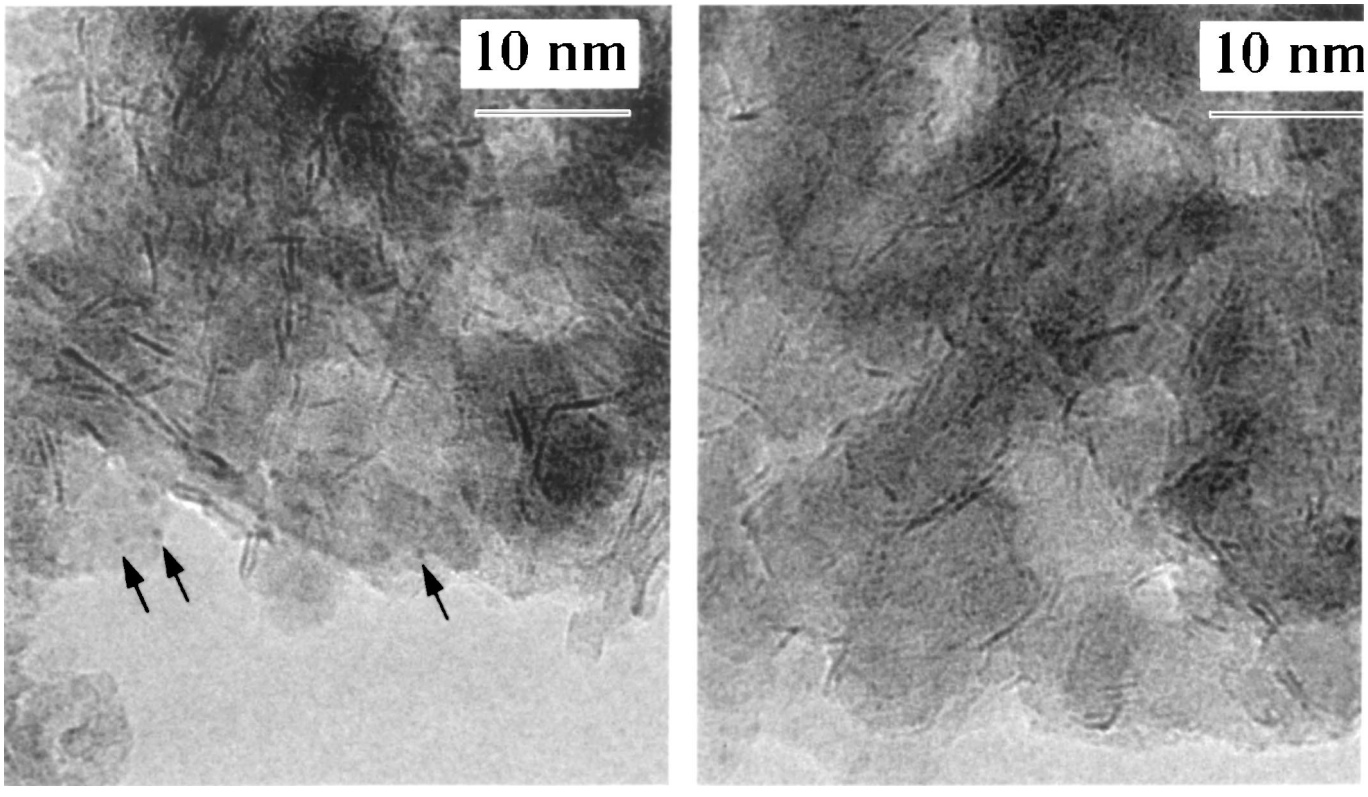

FIG. 7. TEM images of (a) MoS_2 on γ-Al_2O_3 (4.62 Mo/nm^2) and (b) $MoS_2/TiO_2/\gamma$-Al_2O_3 (6.23 Mo/nm^2). The arrows indicate the positions of small particles attributed to unsulfided Mo.

of reduction that is higher than the actual value, and the true extent of reduction for high Mo loadings on TiO_2/γ-Al_2O_3 and would be greater than that on γ-Al_2O_3. (Note that the formation of observable 1-nm particles during TEM does not necessarily imply that the phase from which these particles form cannot consist of substantially larger particles.)

CONCLUSIONS

This work confirms reported differences in activity trends between γ-Al_2O_3 and TiO_2 and conclusively demonstrates that these differences do not arise from different MoS_2 morphologies, i.e., basal plane vs bookend adsorption geometries. TEM images of MoS_2 supported on γ-Al_2O_3 and TiO_2/γ-Al_2O_3 exhibit identical MoS_2 morphologies, even though activity trends differ radically. Instead, the formation of an inactive Mo species at low coverages has been proposed to explain an observed maximum in HDS activity with Mo coverage on γ-Al_2O_3.

The physical processes leading to formation of inactive Mo species on γ-Al_2O_3 surfaces have been demonstrated to arise through the interaction of molybdate precursors with type I-a hydroxyl groups. These hydroxyl groups, identified as being singly bound to tetrahedrally coordinated aluminum cations, can be eliminated either through the use of α-Al_2O_3 supports, or by preferential reaction with titanium alkoxides to form a partial titania overlayer. FTIR results conclusively demonstrate the removal of type I-a hydroxyls by the TiO_2 overlayer and the subsequent reaction of molybdate precursors with lower frequency, less basic, hydroxyls. On either α-Al_2O_3 or TiO_2/γ-Al_2O_3, the formation of inactive Mo species, identified by resistance to reduction as measured by XPS, is minimized. As a result, HDS activity trends shift from exhibiting a maximum in activity with Mo coverage, to a monotonic decrease in activity with coverage. Furthermore, the activities at all coverages are greater on the α-Al_2O_3 and TiO_2/γ-Al_2O_3 supports than on pure γ-Al_2O_3. Overall, this work demonstrates the realization of significant improvements in the performance of γ-Al_2O_3 supported MoS_2 catalysts through a simple, practical modification of the γ-Al_2O_3 support prior to Mo loading.

REFERENCES

1. Pratt, K. C., Sanders, J. V., and Christov, V., *J. Catal.* **124**, 416 (1990).
2. Bachelier, J., Tilliette, M. J., Duchet, J. C., and Cornet, D., *J. Catal.* **76**, 300 (1982).
3. Hu, H., Wachs, I. E., and Bare, S. R., *J. Phys. Chem.* **99**, 10897 (1995).
4. Xie, Y.-C., and Tang, Y.-Q., *Adv. Catal.* **37**, 1 (1990).
5. de Beer, V. H. J., van der Aalst, M. J. M., Machiels, C. J., and Schuit, G. C. A., *J. Catal.* **43**, 78 (1976).

6. Srinivasan, S., Datye, A. K., and Peden, C. H. F., *J. Catal.* **137**, 513 (1992).
7. Delannay, F., *App. Catal.* **16**, 135 (1985).
8. Payen, E., Hubaut, R., Kasztelan, Poulet, O., and Grimblot, J., *J. Catal.* **147**, 123 (1994).
9. Knözinger, H., and Ratnasamy, P., *Catal. Rev. Sci. Eng.* **17**, 31 (1978).
10. Ballinger, T. H., and Yates, J. T., Jr., *Langmuir* **7**, 3041 (1991).
11. Diaz, A. L., and Bussell, M. E., *J. Phys. Chem*. **97**, 470 (1993).
12. Basu, P., Ballinger, T. H., and Yates, J. T., Jr., *Rev. Sci. Inst.* **59**, 1321 (1988).
13. Topsøe, N.-Y., and Topsøe, H., *J. Catal.* **139**, 631 (1993).
14. Okamoto, Y., and Imanaka, T., *J. Phys. Chem*. **92**, 7102 (1988).
15. Zingg, D. S., Makovsky, L. E., Tischer, R. E., Brown, F. R., and Hercules, D. M., *J. Phys. Chem*. **84**, 2898 (1980).
16. Luck, F., *Bull. Soc. Chim. Belg.* **100**, 781 (1991).
17. Li, C. P., and Hercules, D. M., *J. Phys. Chem*. **88**, 456 (1984).
18. Greenwood, N. N., and Earnshaw, A., "Chemistry of the Elements." Pergamon, New York, 1984.
19. Srinivassan, S., Datye, A. K., Hampden-Smith, M., Wachs, I. E., Deo, G., Jehng, J. M., Turek, A. M., and Peden, C. H. F., *J. Catal.* **134**, 260 (1991).
20. Kerkhof, F. P. J. M., and Mouljin, J. A., *J. Phys. Chem*. **83**, 1612 (1979).
21. Barringer, E. A., and Bowen, H. K., *Langmuir* **1**, 414 (1985).
22. Reardon, J., "Tailoring Alumina Surface Chemistry for Efficient Use of Supported MoS_2." Masters thesis, Univ. of New Mexico, 1996.
23. Daage, M., and Chianelli, R. R., *J. Catal.* **149**, 414 (1995).
24. Singhal, G. H., Espino, R. L., Sobel, J. E., and Huff, G. A., Jr., *J. Catal.* **67**, 457 (1981).
25. Froment, G. F., and Bischoff, K. B., "Chemical Reactor Analysis and Design," 2nd ed., p. 70. Wiley, New York, 1990.
26. Roxolo, C. B., Daage, M., Rupert, A. F., and Chianelli, R. R., *J. Catal.* **100**, 176 (1986).
27. Singhal, G. H., Espino, R. L., Sobel, J. E., and Huff, G. A., Jr., *J. Catal.* **67**, 457 (1981).
28. Sault, A. G., Boespflug, E. P., and Peden, C. H. F., *J. Phys. Chem*. **98**, 1652 (1994).
29. Sault. A. G., *J. Catal.* **156**, 154 (1995).
30. Wagner, C. D., Six, H. A., Jansen, W. T., and Taylor, J. A., *Appl. Surface Sci.* **9**, 203 (1981).
31. Wagner, C. D., Riggs, W. M., Davis, L. E., Moulder, J. F., and Muilenberg, G. E., "Handbook of X-ray Photoelectron Spectroscopy." Perkin-Elmer Corp., Eden Prairie, MN, 1979.
32. Halada, G., private communication.
33. Kantcheva, M. M., Bushev, W. Ph., and Hadjiivanov, K. I., *J. Chem. Soc. Faraday Trans.* **88**, 3087 (1992).
34. Bohem, H.-P., and Knözinger, H., *in* "Catalysis—Science and Technology" (J. R. Anderson and M. Boudart, Eds.), Vol. 4, p. 49. Academie-Verlag, Berlin, 1983.
35. Park, G. A., *Chem. Rev.* **65**, 177 (1965).
36. Patterson, T. A., Carver, J. C., Leyden, D. E., and Hercules, D. M., *J. Phys. Chem*. **80**, 1700 (1976).